Final Research Report

Stanford Electronics Lab JESP Contract

J. S. Harris
Principal Investigator and Director

March 31, 2001

U. S. Army Research Office
DAAG55-97-1-0115

Stanford University

**Approved for Public Release
Distribution Unlimited**

The views, opinions and/or findings contained in this report are those of the author and should not be construed as an official Department of the Army position, policy or decision unless designated by other documentation.

1

Abstract

This is the final report of the research conducted at Stanford Electronics Laboratories under the sponsorship of the Joint Services Electronics Program from March 1, 1997 through March 31, 2001. This report summarizes the areas of research, identifies the most significant results and lists the dissertations, publications and presentations sponsored by the contract (DAAG55-97-1-0115).

Key Words and Phrases: None

Table of Contents

Introduction

This report summarizes the activities in the research programs at the Stanford Electronics Laboratories sponsored by the Joint Services Electronics Program under contract DAAH04-94-G-0058. This contract is monitored by the Army Research Office, Research Triangle Park, North Carolina.

This report covers a four year wind down period after 50 years of the JSEP program at Stanford. This period of research supported only students who had been previously supported to enable them to complete their PhD degrees without switching research topics

INVESTIGATION OF FABRICATION AND TRANSPORT IN QUANTUM DOTS

PRINCIPAL INVESTIGATOR: J. S. Harris, Jr.
GRADUATE STUDENTS: B. Shimbo and D. Stewart

1. Scientific Objectives

Present semiconductor devices and ICs are based upon classical charge transport in semiconductors. As device dimensions continue to shrink, they are rapidly approaching the size scale where the quantum effects of charge quantization, electron-electron interaction and quantum interference dramatically affect the device behavior. The physical rules governing charge transport are fundamentally different on the two sides of this size boundary: for larger devices the familiar classical, collective charge models presently used work very well; for smaller devices classical models break down and predict inaccurate or totally incorrect behavior. Both fabrication techniques and an understanding of the quantum charge transport will be necessary to realize new device and IC designs in this nano-size regime.

We have conducted an investigation into the quantum charge transport of individual quantum dot (QD) devices. Our two main objectives in this work were: 1) to investigate experimentally the impact of electron-electron interactions on charge transport through a quantum dot and 2) to investigate new fabrication techniques that might be applicable to realize single electron devices.

2. Significant Progress

In a typical SET design, the central island is defined by tunneling barriers to the source and drain leads. Many of the first SETs featured vertical tunneling junctions fabricated using electron beam lithography and shadow evaporation techniques.[2] Although thin oxide tunneling barriers narrower than 100 nm are readily produced by vertical junctions, lateral tunneling junctions offer certain advantages. The possibility of reduced capacitances due to smaller lateral junction areas should lead to higher possible operating temperatures. Furthermore, the lateral configuration lends itself to easier integration with other planar devices. We have been investigating two methods for the fabrication of lateral metal-insulator-metal tunneling barriers, atomic force microscope (AFM) oxidation and current-induced local oxidation (CILO).

The AFM is typically used to image surface features almost atomic resolution. The key element of the AFM is an atomically sharp tip suspended from the end of a cantilever. In contact mode, the tip rides over features as it traverses the surface in a raster pattern. A feedback circuit maintains a constant cantilever deflection by adjusting the height of the sample with a

piezoelectric stage. Conductive AFM tips can be made by fabricating the tips out of doped Si, or by coating standard Si or SiN tips with metal films.

AFM oxidation is accomplished by applying an electrical bias between a conductive AFM tip and a thin film, which locally anodizes the film, using surface adsorbed water as an electrolyte.[3] Translating the tip across the film surface while applying a bias produces oxide lines with widths ranging from tens to hundreds of nanometers.

We studied the AFM oxidation process by investigating various conductive tips, semiconductor and metal films, and oxidation parameters. Thin films of Ti, Ni, and Cr were applied to the AFM tips in an electron beam evaporator. The coated tips were studied for wear and film adhesion with a scanning electron microscope. Commercially available conductive Si and PtIr-coated tips were also used and compared.[4]

A number of materials were also studied as candidates for substrate material. Thin metal films were evaporated or sputtered onto 100 nm of thermally grown SiO_2. Molecular beam epitaxy (MBE)-grown films of GaAs and NiAl were also used. The NiAl film seemed to have particular promise for excellent oxide line uniformity due to its single-crystal structure and very flat surface.[5] Furthermore, the aluminum oxide produced had potentially strong physical and electrical traits. Unfortunately, the NiAl film proved difficult to oxidize and the GaAs substrate on which the NiAl was grown provided poor isolation. The investigation then focused on electron-beam evaporated films of Ti with thicknesses ranging from 3 to 10 nm.

We studied control over the oxide linewidth by varying the AFM tip translation speed and the applied voltage. We found that the linewidth could be reduced by increasing the tip translation speed and lowering the applied voltage. Oxidation would not proceed, however, if the speed was raised or the voltage dropped beyond a certain point. Importantly, the width of the oxide line was also found to be sensitive to the ambient humidity, the shape of the AFM tip, and local surface conditions. The oxide height is determined by the thickness of the film. In the case of Ti, the oxide occupies roughly twice the volume of the original metal, so a TiOx line that completely cut through a 3 nm Ti film would extend about 3 nm above the surface.

For device fabrication, the Ti films were patterned using contact photolithography and a wet etching process in HF to create large-scale two or three-terminal structures consisting of a 2 μm-wide line or T-junction, respectively. We used the AFM to define sub-micron features and attempted many different structures, investigating the capabilities of both AFM oxidation in general, and the translation capabilities of our specific AFM. Hysteresis and drift in the piezoelectrics controlling the motion of the AFM had to be accounted for in the software scripts that directed the movement. Broad oxide lines drawn at low speeds and high biases were used to provide electrical isolation and to define certain device features. High speeds and low biases produced fine oxide lines for use as lateral tunneling barriers. Figure 1 is an AFM image of a device fabricated with AFM oxidation.

The electrical barrier height of the oxide barriers was determined by taking current-voltage measurements in a cryostat from 200 K to room temperature. Plotting the current versus temperature at different bias points, we extract activation energies. We account for the image force barrier lowering by plotting the activation energies versus the square root of the bias and extrapolate back to zero volts. Contact difficulties limited the number of devices that could be tested. A barrier height of 0.126 eV was measured for the device shown in Figure 2.
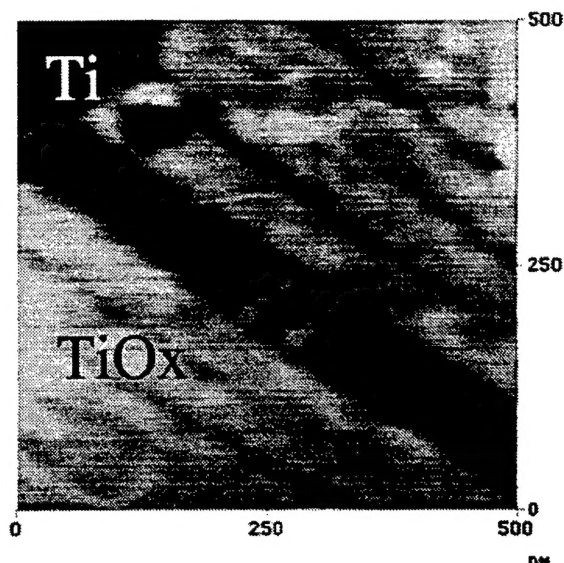
Figure 1. AFM image of a structure made with AFM oxidation. The dark gray is Ti and the light gray is TiOx extending about 3 nm above the Ti surface. The broad oxide lines on the sides were drawn first under low speed, high bias conditions. The two narrow lines in the center were drawn at higher speed and lower bias.

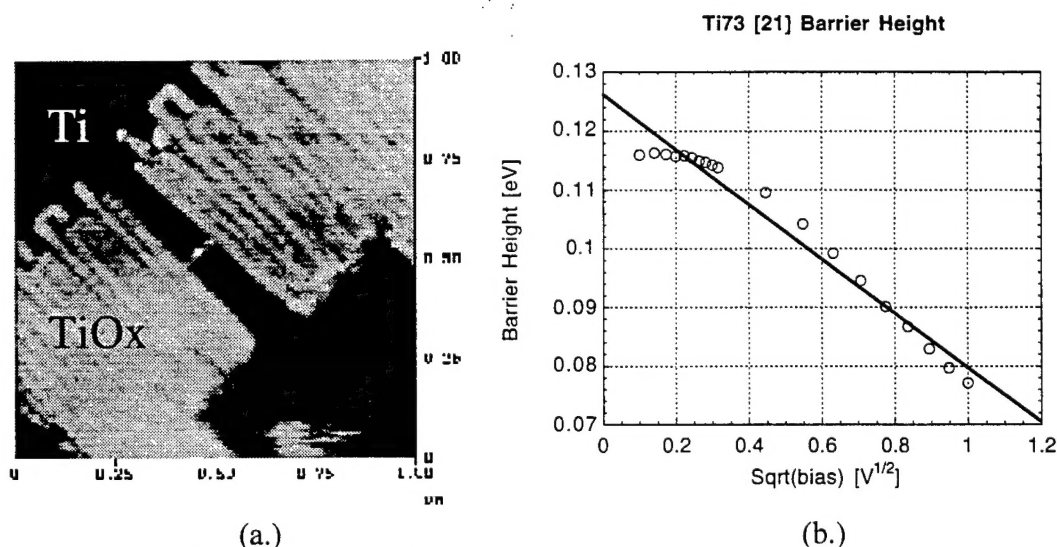
(a.)   (b.)

Figure 2. a.) AFM image of single barrier made with AFM oxidation. b.) Zero bias barrier height of 0.126 eV measured.

Challenges with the reproducibility of the AFM oxidation process lead us to consider alternative methods for the fabrication of lateral tunneling barriers. Current-induced local oxidation, which generates oxides at narrow constrictions in conductor lines, appeared to be a promising candidate.[6] CILO takes advantage of the local high current density produced in a constriction. The early stages of electromigration damage enhance diffusion of oxygen into the metal film, increasing the oxidation rate in the constriction. Joule heating also increases oxygen diffusivity and the oxidation reaction rate. A narrow oxide line quickly grows from the film surface down to the insulating substrate. At this point, the current falls dramatically, and the

5

process naturally halts itself. A plot of the current during the CILO process is shown in figure 3. Initially, the current changes very little as the resistance is dominated by the leads. As the oxide extends deeper and deeper into the metal film, the contribution of the constriction to the total resistance soon begins to be evident. Finally, the metal line is pinched off and the current passes entirely through the barrier.
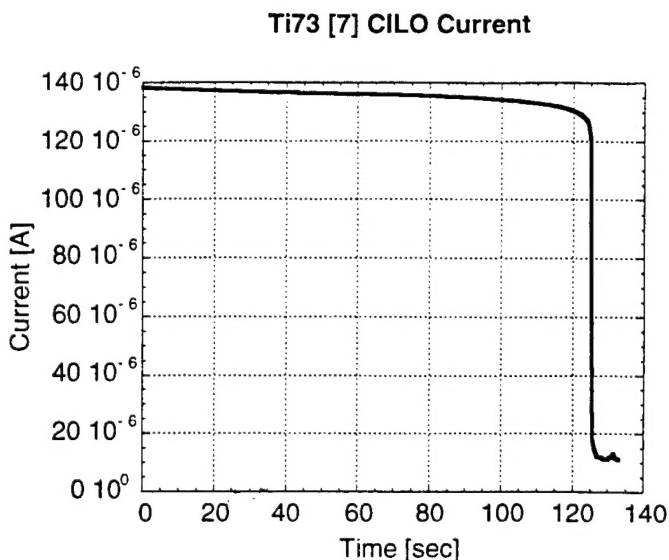
Ti73 [7] CILO Current

Figure 3. Plot of the current through the CILO process. As the oxide grows into the metal film, the current is confined to a narrower and narrower portal. After the oxidation is complete, all remaining current passes through the oxide barrier.

We began investigating CILO with a hybrid AFM-CILO process in which we used the same patterned Ti films fabricated for AFM oxidation. We used AFM oxidation to define sharp and narrow constrictions in 2 μm wide Ti lines. Applying biases up to 20 V across these lines produced current densities greater than 10^7 A/cm^2, and oxidation took place in the gap. An AFM image of the CILO oxide and a plot of the current-voltage characteristic before and after CILO are shown in figure 4. The barrier height of this CILO oxide was also determined in the same way as the AFM oxides, and was found to be 0.119 eV.

To improve the reproducibility of the constrictions and ease their fabrication, we began to focus on using electron beam lithography and lift-off to form the initial constrictions, instead of AFM oxidation. We developed a process to achieve 150 nm resolution using a diluted ZEP520 resist followed by electron beam evaporation. Lift-off was performed in resist stripper while in an ultrasonic bath.

The CILO process remains poorly understood, however. We seek to investigate the relative importance of the electromigration and heating enhancements of the oxidation. Since grain boundary diffusion generally dominates in thin films, we will investigate the influence of the metal film grain size on CILO, and hence the role of the diffusion of vacancies along grain boundaries. Samples from different evaporators and samples that have undergone different periods of annealing will have different grain sizes and may react differently to the CILO

process. We will also investigate the Joule heating to determine how hot the temperature in the gap is relative to its surroundings.
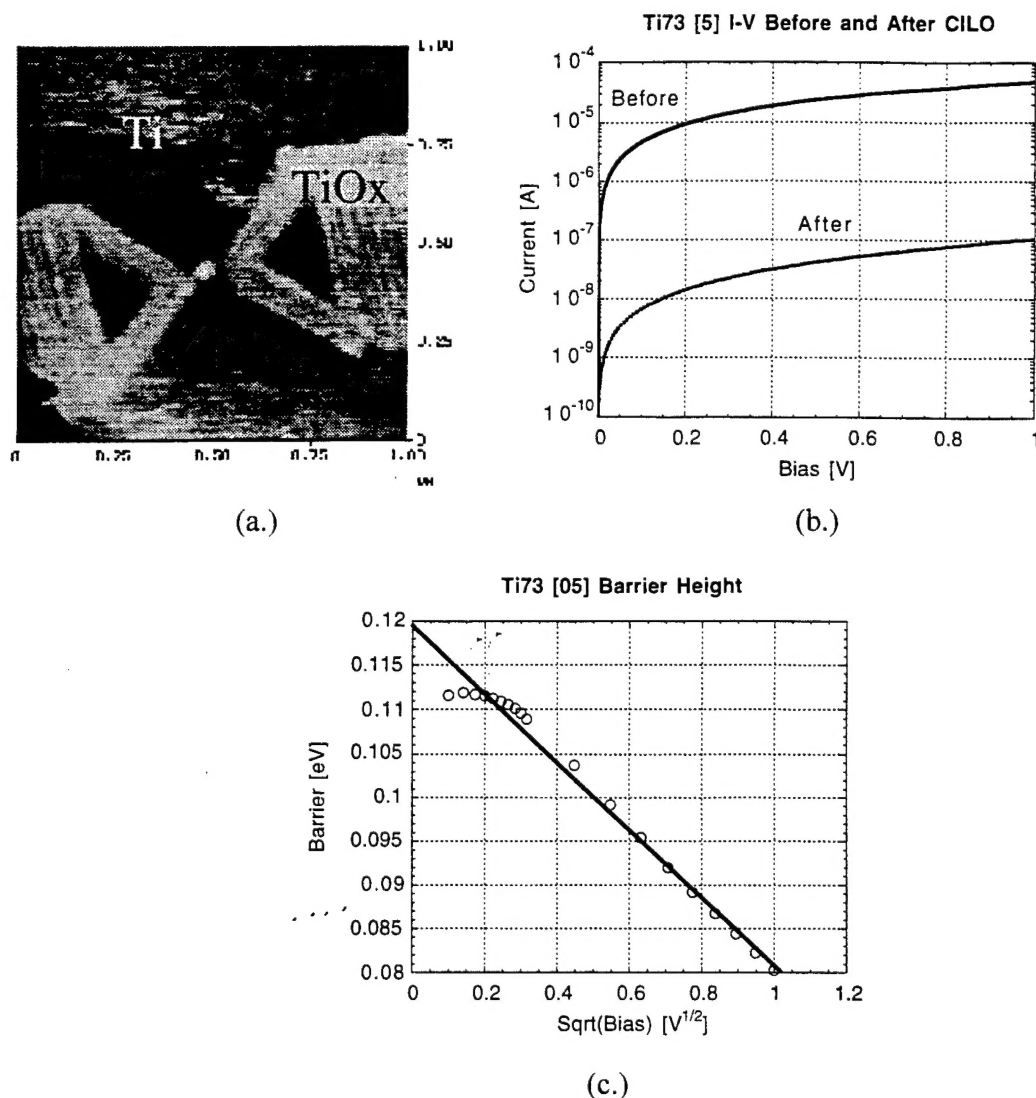

(a.)

(b.)

(c.)

Figure 4. a.) AFM image of CILO oxide generated in gap formed by AFM oxidation. b.) Plot of the current-voltage characteristic before and after CILO. c.) Zero bias barrier height of 0.119 eV measured.

The improved understanding of CILO will be useful for its application to single electron device fabrication. Single CILO barriers may be used as tunneling barriers in SETs, but this would require very narrow oxide lines. We propose a novel use that has less stringent fabrication requirements. A layer of Au could be deposited prior to the evaporation of Ti. When less than a nanometer of Au is deposited, the Au tends to clump into islands. With a reasonably sparse distribution, a small number of islands will be found directly in the constriction formed in the Ti line. A CILO oxide can then be formed to isolate the Au island. In this device, electrons tunnel through only a part of the barrier, and a single line acts as both source and drain tunnel

junctions. This eases the requirement that lines must be made as thin as possible to allow tunneling. A schematic of the proposed device is shown in figure 5.
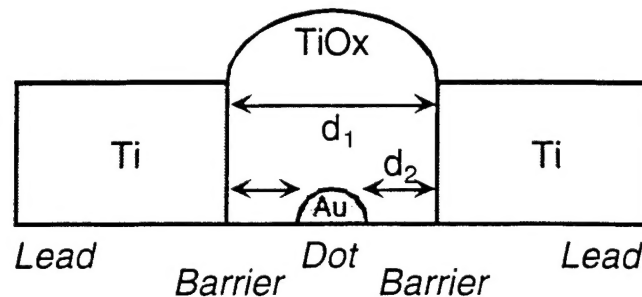

Figure 5. Side view schematic of proposed device using CILO to isolate Au islands. The linewidth requirement is eased since d_2 is now the tunneling distance instead of d_1.

3. References

1. K. K. Likharev, IBM J. Res. Develop. **32**, 144 (1988).
2. T. A. Fulton and G. J. Dolan, Phys. Rev. Lett. **59**, 109 (1987).
3. K. Matsumoto, M. Ishii, K. Segawa, Y. Oka, B. J. Vartanian, and J. S. Harris, App. Phys. Lett. **68**, 34 (1996).
4. Conductive Si tips were purchased from Park Scientific Instruments. PtIr tips were purchased from Nanosensors.
5. C. Y. Hung, M. V. Weckwerth, A. F. Marshall, Y. C. Pao, and J. S. Harris, Journal of Crystal Growth **169**, 201 (1996).
6. Ph. Avouris, R. Martel, T. Hertel, and R. Sandstrom, Applied Physics A **66**, pp. S659-S667 (1998).

4. JSEP Supported Publications

1. D. R. Stewart, D. Sprinzak, C. M. Marcus, C. I. Duruöz and J. S. Harris, Jr., *Science* **278**, 1784 (1997).
2. S. R. Patel, S. M. Cronenwett, D. R. Stewart, A. G. Huibers, C. M. Marcus, C. I. Duruöz, J. S. Harris, K. Campmana and A. C. Gossard, *Phys. Rev. Lett.* **80**, 4522 (1998).
3. K. L. McCormick, M. T. Woodside, M. Huang, P. L. McEuen, C. I. Duruoz, J. S. Harris, Jr., "Scanned potential microscopy of a two-dimensional electron gas" *Physica B*, **251** pp. 79-83 June 1998
4. C. M. Marcus, S. R. Patel, C. I. Duruoz, J. S. Harris, Jr., K. Campman, A. C. Gossard, "Statistics of peak spacings and widths in the quantum coulomb blockade regime" *Physica B*, **251** pp. 201-205 June 1998
5. G. S. Solomon, W. Wu, J. R. Tucker, J. S. Harris, Jr, "Vertical InAs diffusion and surface ordering processes in InAs vertical quantum dot columns" *Physica E*, **2** (1-4) pp. 709-713 July 1998
6. A. G. Huibers, S. R. Patel, C. M. Marcus, P. W. Brouwer, C. I. Duruöz and J. S. Harris, Jr., "Distributions of the Conductance and its Parametric Derivatives in Quantum Dots", *Phy. Rev. Lett*, **81** (9) pp. 1917-1920 Aug. 1998.
7. S. R. Patel, D. R. Stewart, C. M. Marcus, M. Gökcedag, Y. Alhassid, A. D. Stone, C. I. Duruöz and J. S. Harris, Jr., "How Adding Electrons Scrambles the Electronic Spectrum of a Quantum Dot",

8.   S. R. Patel, S. M. Cronenwett, D. R. Stewart, A. G. Huibers, C. M. Marcus, C. I. Duruöz, J. S. Harris, Jr., K. Campman, and A. C. Gossard, "Statistics of Coulomb Blockade Peak Spacings", *Phy. Rev. Lett.* **80**, 4522-4525, May, 1998.

9.   S. M. Cronenwett, S. M. Maurer, S. R. Patel, C. M. Marcus, C. I. Duruoz, J. S. Harris, Jr.,"Mesoscopic Coulomb blockade in one-channel quantum dots," *Phys. Rev. Lett.* **81** (26) pp. 5904-5907 Dec. 1998

10. S. R. Patel, D. R. Stewart, C. M. Marcus, M. Gokcedag, Y. Alhassid, A. D. Stone, C. I. Duruoz, J. S. Harris, Jr., "Changing the electronic spectrum of a quantum dot by adding electrons," *Phys. Rev. Lett.* **81** (26) pp. 5900-5903 Dec 1998

11. K. Matsumoto, Y. Gotoh, T. Maeda, J. A. Dagata, J. S. Harris, Jr., "Metal-based room-temperature operating single electron devices using scanning probe oxidation," *J. J. Appl. Phys.* **38** (1B) pp. 477-479 Jan. 1999

12. Y. Okada, Y. Iuchi, M. Kawabe, J. S. Harris, Jr., "An AlGaAs/GaAs tunnel diode integrated with nanometer-scale atomic force microscope tip-induced oxides" *Japanese .J. Appl. Phys. Part 2-Lett.*, **38** (2B) pp. L160-L162 Feb. 1999

13. McCormick KL, Woodside MT, Huang M, Wu MS, McEuen PL, Duruoz C, Harris JS, "Scanned potential microscopy of edge and bulk currents in the quantum Hall regime," *Phys. Rev B* ,**59** (#7) pp. 4654-4657, (1999)

14. S. M. Maurer, S. R. Patel, C. M. Marcus, C. I. Duruoz, J. S. Harris, Jr., "Coulomb blockade fluctuations in strongly coupled quantum dots" *Phys. Rev. Lett.* **83** (7) pp. 1403-1406 Aug. 1999.

15. G. Huibers, J. A. Folk, S. R. Patel, C. M. Marcus, C. I. Duruoz, J. S. Harris, Jr., "Low-temperature saturation of the dephasing time and effects of microwave radiation on open quantum dots" *Phys. Rev. Lett.* **83** (24) pp. 5090-5093 Dec. 1999

16. K. Matsumoto, Y. Gotoh, T. Maeda, J. A. Dagata, J. S. Harris, Jr., "Room-temperature single-electron memory made by pulse-mode atomic force microscopy nano oxidation process on atomically flat alpha-alumina substrate" *Appl. Phys. Lett.* **76** (2) pp. 239-241 Jan. 2000

5. JSEP supported doctoral theses

1.   D. R. Stewart, "Level spectroscopy of Quantum Dots", Stanford University (1998).

**TITLE: Physics Technology and Applications of Ultra-small Structures**
PRINCIPAL INVESTIGATOR: R. F. W. Pease
GRADUATE STUDENTS: T. Kramer and K. Gilbert

The Micromachined Tunneling Transistor (MTT)

The focus of this work is the simulation, fabrication, and testing of a Micromachined Tunneling Transistor (MTT). The MTT, as shown in Fig 1, consists of a micromachined relay that is used to bring two gold surfaces to within several nanometers of one another. When the two surfaces are this close, electrons can tunnel from one surface to the other. This tunneling current can be modulated by slight movements of the relay, with one angstrom of relay movement corresponding to a 2X change in tunneling current. The modulation of the width of the tunneling barrier is potentially much more efficient than the standard MOSFET, which modulates the height of a potential barrier.

Fig 1 Micromachined Tunneling Transistor
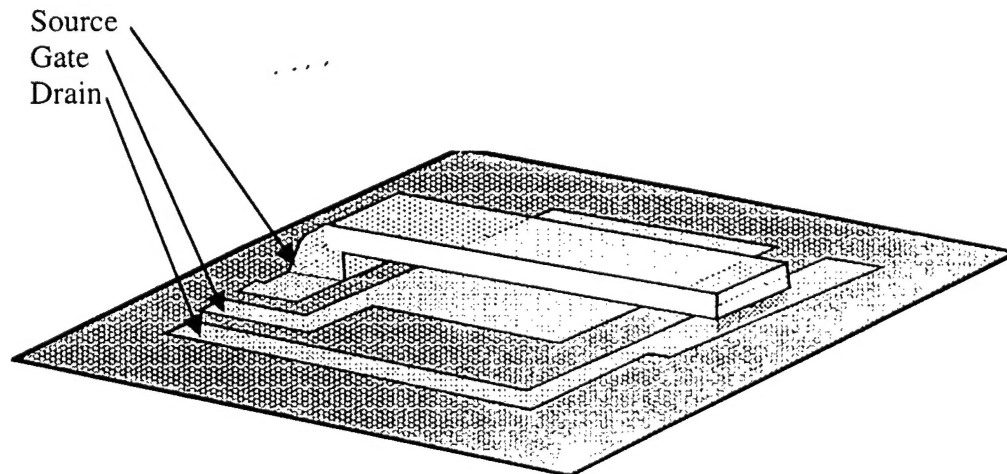
The recent focus of the MTT project has been on fabrication and testing of the MTT. Despite the design of particularly robust hinge structures, initial fabrication attempts invariably resulted in structures that were stuck down to the substrate. This problem was solved by using a Critical Point Drier (CPD) for the final release step.

We have tested several different configurations of the MTT. Figure 2 shows the tips of a lateral unit that was created using the MUMPS/Cronos fabrication process. These lateral tunneling units exhibit are actuated using comb drive structures. The actuation mechanics of a comb drive structure eliminate the pull-in instability that is a problem in the classic relay devices. However, the lateral unit is subject to out-of-plane forces, and these have kept us from establishing continuous tunneling contact in the MUMPS devices. Lack of funding and progress on other fronts made a second revision of the design impossible.
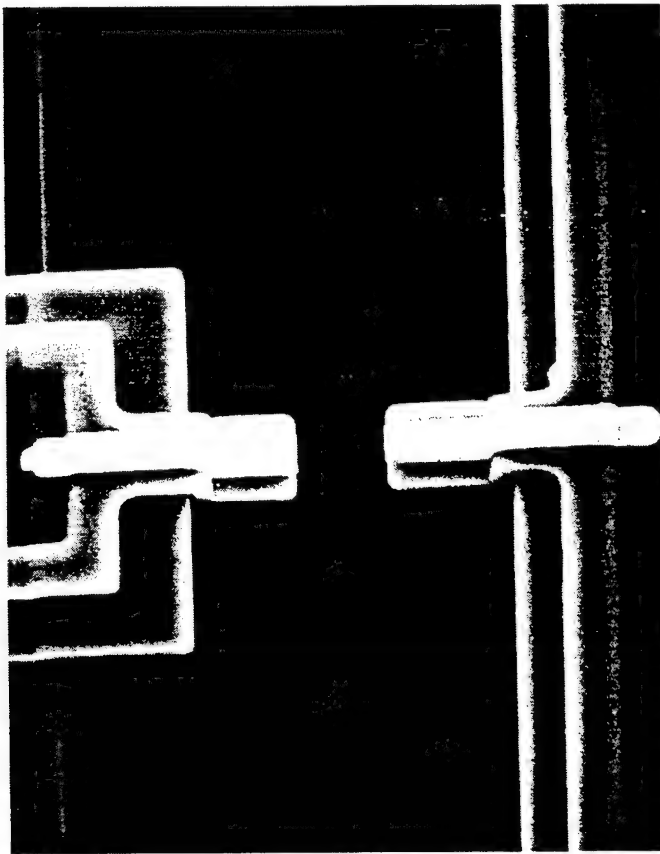

Figure 2: Lateral Unit

The most successful MTT configuration has been the dual anchor lever, shown in figure 3. The dual anchor devices are more robust and thus survive the processing in greater numbers. They are also stiffer, which limits their gain and increases actuation voltages.
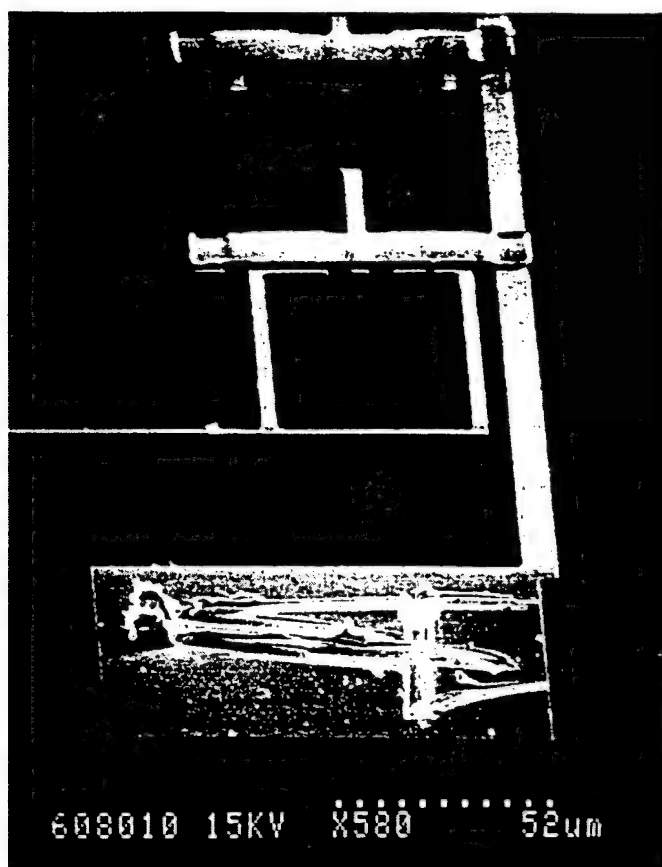
Fig 3: Dual anchor (with bonding pad in foreground)

The dual anchor devices exhibit the classic relay problem of pull-in. Thus we implemented several different methods of stabilization for these devices. The first method was leveraged bending, where the length of the gate electrode is shortened until the tip of the lever can be actuated smoothly over the full range of motion of the device. Several of the dual anchor devices using this method have exhibited tunneling current, showing that they have full range actuation. The IV curve of a device with a very small pull-in height (and thus nearly stable full-range) is show in figure 4. The curve shows only a 4-volt hysteretic loop, an order of magnitude lower than that predicted for a full-gate device of the same dimensions. These devices are still under testing.
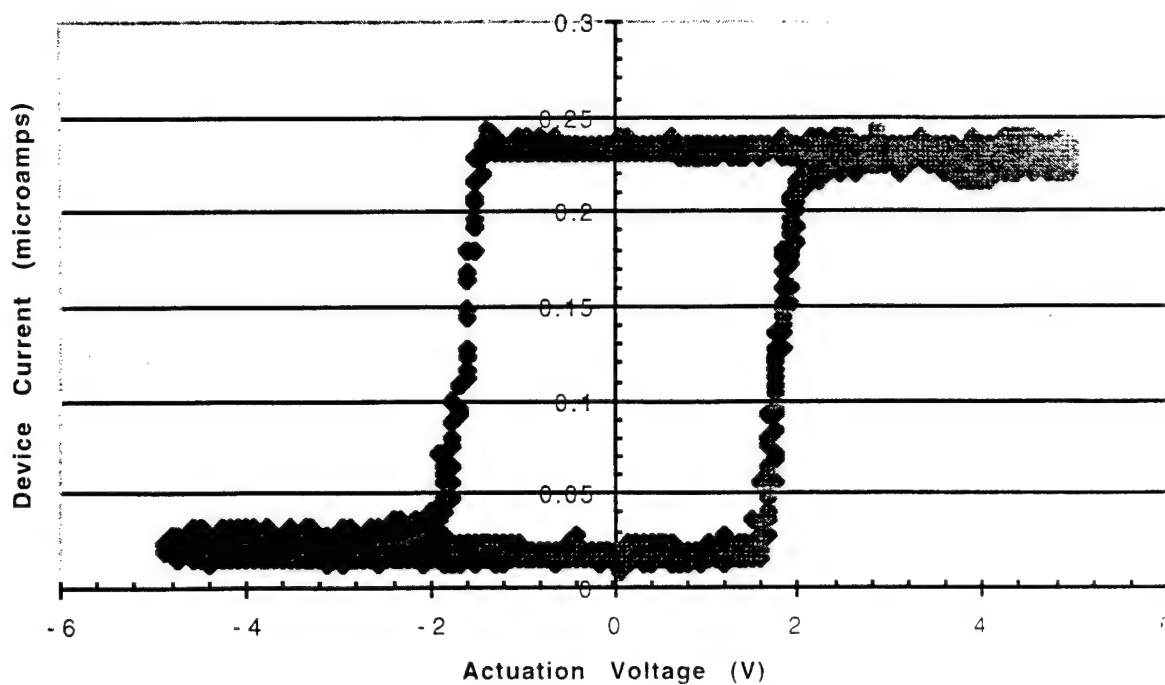
The second method of stabilization implemented for the dual anchor devices is a raised drain. In this method, the drain of the device is raised far enough so that it enters the range of stable motion of the device. A scanning electron microscope (SEM) picture of such a device is shown in Fig 5. These device have initial source-drain gaps of as little as 0.1 microns, and have been actuated several thousand times. We are currently working on a new revision of electronics that will allow these devices to tunnel without actuating them to failure.
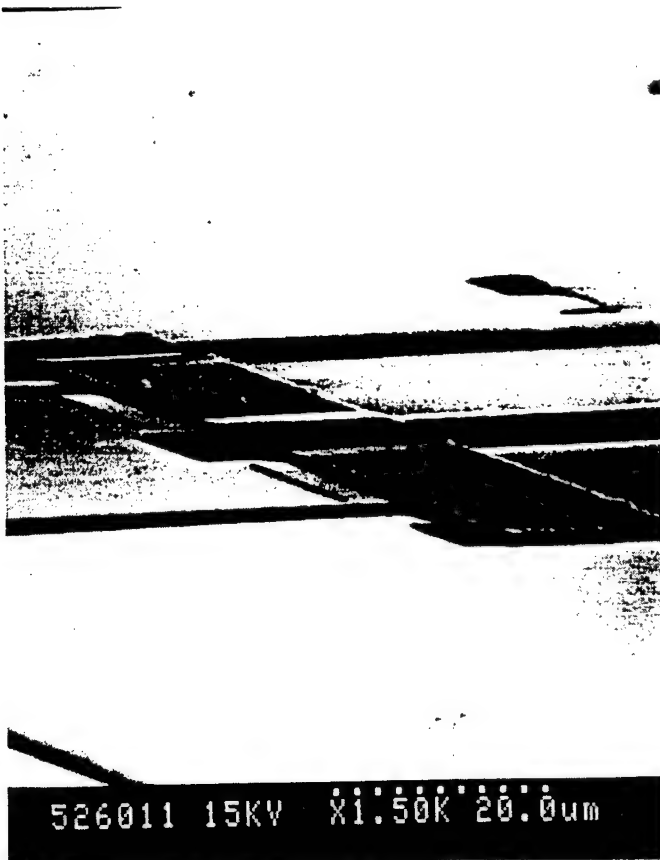
526011 15KV X1.50K 20.0um

Fig 5: Raised Drain

Electrical Properties of Sub 100 nm Silicon Structures

Semiconductor device dimensions are rapidly shrinking into the far sub-micron regime. As dimensions reach the order of 100 nm, the low frequency noise, which is generated by the interaction of channel carriers with nearby traps in the gate oxide, can no longer be described by the characteristic 1/f spectrum.[Hung, Jayaraman] At this scale, the effects of individual traps are visible as random telegraph signals in the room temperature channel conductance.[Kirton] Devices with a single trap active in the measurement range have been extensively studied in the literature, but the possibility of a "zero-trap" device, one with no low frequency noise due to traps, has received minimal attention. This research investigates the low frequency noise sources underlying the trap noise through the study of two types of surrounding-gate transistors. The first, a cylindrical surrounding-gate transistor, is used to assess the possibility of a "zero-trap" device because its small channel area, 0.1 um length by 0.16 um width, is predicted to have an average of 0.5 active traps per device. The second device, a depletion-mode far surrounding-gate transistor, is used to drive the current away from the oxide traps while the noise spectrum is measured. Fabrication and preliminary electrical characterization of both devices has been completed.

The cylindrical surrounding-gate transistor is a vertical transistor built from a silicon nanopillar. Nanopillars are fabricated by using electron beam lithography, plasma etching, and self-limiting oxidation to form a p-type silicon core 730 nm tall and less than 50 nm wide. Gate oxidation and gate polysilicon deposition follow. The surrounding-gate is formed with a spacer etch, and the source and drain at the bottom and top of the pillar are doped with an angled implant. The whole structure is passivated with deposited oxide and vias are etched to the source and gate and filled with deposited metal. Electrical contact to the top of the pillar is accomplished by the use of a focused ion beam to first etch a hole to the top of the pillar and then deposit a tungsten plug. An SEM image of the cross section of the device following passivation is shown in Figure 1a. An FIB image of the cross section of the finished device showing etched top via and tungsten plug is show in Figure 1b.
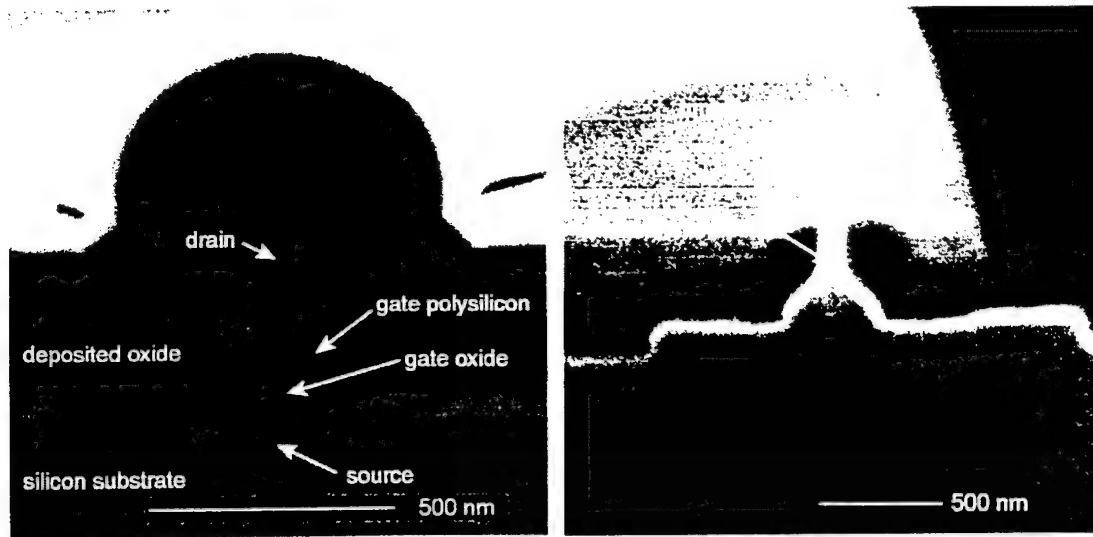
Figure 1: a) SEM image of cylindrical surrounding-gate transistor cross section showing 50 nm wide silicon nanopillar with surrounding gate. Source and drain are doped at top and bottom of pillar. b) FIB image of cylindrical surrounding-gate transistor cross section showing FIB etched top via filled with tungsten plug.

The DC electrical characteristics of a single cylindrical surrounding-gate transistor show gate modulation of the drain current. The device is biased and measured using the source/monitor units of an HP4145B semiconductor parameter analyzer. The substrate and source are grounded while the drain voltage is swept and the gate voltage is stepped. An Id-Vd sweep for a single device is shown in Figure 2.

Figure 2: Drain current versus drain voltage at various gate voltage steps for a cylindrical surrounding-gate transistor.

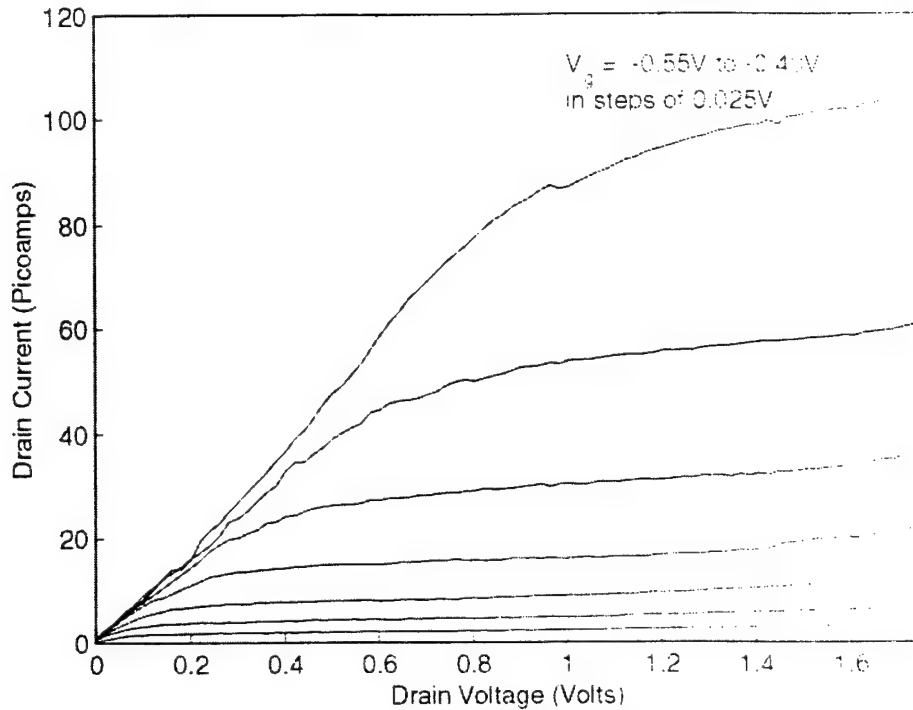Noise measurements will be taken in the time domain by amplifying the fluctuations in the drain current at fixed gate and drain bias and measuring them on an oscilloscope. For a single active trap, these fluctuations will take the form of a random telegraph signal with the trap switching between a filled and empty state. As the device is biased away from the trap such that the trap is no longer active, the noise due to underlying sources will become visible as the random telegraph signal amplitude falls below that of the underlying noise.

The depletion-mode fin surrounding-gate transistor, rather than being cylindrically symmetric, is elongated in one lateral direction. Aside from the elongated dimension and the channel doping, this device shares the same fabrication steps with the cylindrical surrounding-gate transistor. A diagram of the depletion-mode fin surrounding-gate transistor is shown in Figure 3a and an SEM image of a gated depletion-mode fin surrounding-gate transistor is shown in Figure 3b.
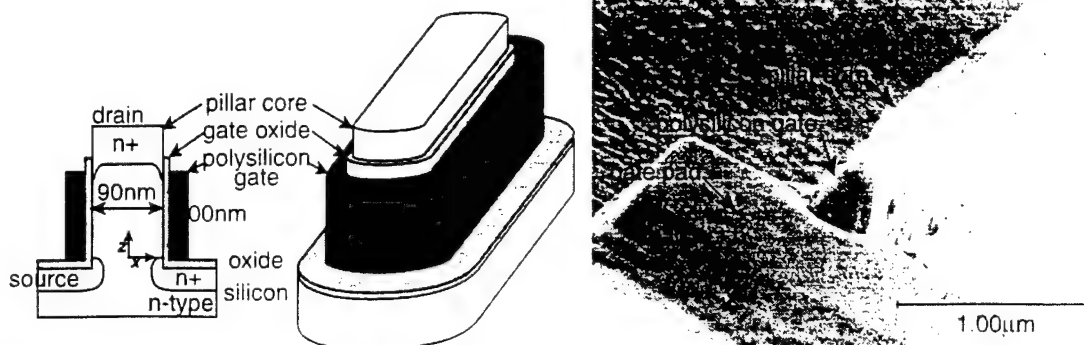
Figure 3: a) Diagram of depletion-mode fin surrounding-gate transistor b) SEM ... in oblique view of gated depletion-mode fin surrounding-gate transistor before passivation.

The low frequency (1/f) noise spectrum of depletion-mode fin surrounding-gate transistors will be measured as the gate bias forces electrons away from the interface. Noise remaining when electrons no longer interact with the surface will be due to the non-surface low frequency noise sources to be studied. While no studies of devices with this geometry and size have been reported in the literature, a study by Amberiadis and van der Ziel shows that as the conducting region in large area MOS capacitors is forced away from the silicon/silicon dioxide interface, the magnitude of the 1/f noise decreases.[Amberiadis]

References

[Amberiadis]   K. Amberiadis and A. van der Ziel, *Solid-State Electron.*, **26**, 1009 (1983)

[Hung]   K. K. Hung, P. K. Ko, C. Hu, and Y. C. Cheng, *IEEE. Trans. Electron Dev.*, **37**, 654 (1990).

[Jayaraman]   R. Jayaraman and C. G. Sodini, *IEEE Trans. Electron Devices*, **36**, ... (1989).

[Kirton]   M. J. Kirton and M. J Uren, *Adv. Phys.*, **38**, 367 (1989).

FIBER-BASED OPICAL FREQUENCY CONVERSION: A NOVEL DEVICE AND WDM NETWORK APPLICATIONS

PRINCIPAL INVESTIGATOR: Leonid. G. Kazovsky

RESEARCH STUDENT: Min-Chen Ho

1 INTRODUCTION

Wavelength converters are important building blocks in WDM networks. They allow non-blocking wavelength routing and de-centralized wavelength management [Yoo] [Willner]. Although wavelength converters based on O/E/O techniques provide good signal quality, all-optical wavelength converters have the advantages of modulation format and bit-rate transparency, and can provide multi-wavelength conversion simultaneously. Several all-optical wavelength conversion techniques have been proposed and demonstrated [Stubkjaer] [Brener] [Watanabe] [Aso]. Fiber-based optical wavelength converters (FWCs) utilizing the parametric amplification in fibers are also all-optical wavelength converters. Besides the common benefits that all-optical wavelength conversion techniques can provide, FWCs can potentially have high gain and wide bandwidth [Marhic-a]. Recent research efforts in WDM system show interest in wavelength regions outside the conventional EDFA band, i.e., L-band [Sun] and S-band [Kani], in order to increase transmission capacity in optical fiber. FWCs' potential wide bandwidth would help meet the future need of WDM systems.

During the first year of our project (May 1st, 1997 – December 31st, 1997), we have performed theoretical and experimental studies of one-pump and two-pump FWC. During the second year (Jan 1st, 1998 – December 31st, 1998), the main focus of our research was to develop techniques to further increase the operating bandwidth of FWC. During the third year (Jan 1st, 1999 – December 31st, 1999), we have continued the effort in developing wideband FWCs and studied the interaction of FWCs with other nonlinear phenomena in fibers, i.e., stimulated Raman scattering. We spent the remaining period of this project (Jan 1st, 2000 – March 31st, 2001) developing FWCs for practical system application. We proposed and demonstrated a method using two pumps for suppressing idler linewidth broadening.

Section 2 summarizes the research achievement supported by this project. This project directly supported six conference publications, four journal publications, and one

Ph. D. dissertation. which will be published in June 2001. Sections 3 and 4 list the titles of the publications and the dissertation.

2   SUMMARY OF RESEARCH RESULTS

Highly nonlinear dispersion-shifted fiber (HNLF) is a key component in this project. Its high nonlinearity and flat dispersion slope help to increase the conversion efficiency. and reduce the fiber length required to achieve a certain wavelength conversion efficiency. Section 2.1 introduces HNLFs and describes an FWC constructed with an HNLF.

Although HNLFs have the desired features for making FWCs. their zero-dispersion wavelengths are not easy to control during manufacturing due to the small core size. We have proposed and demonstrated a periodic compensation technique to overcome this problem. Section 2.2 summarizes the results of this technique.

Theory shows that the bandwidth of FWCs using HNLF could be over 200 nm. Under these circumstances the FWC bandwidth would overlap the pump-induced Raman gain bandwidth. We have studied the combined effects of FWC and Raman gain theoretically and experimentally. Section 2.3 shows experimental results for a 200 nm-bandwidth FWC. and summarizes the influence of the Raman effect encountered in our studies.

The performance of cw-FWCs has been hampered by pump-induced converted-signal spectrum broadening. due to the required pump phase modulation. We theoretically investigate and experimentally demonstrate a technique to cancel the idler (converted-signal) broadening by using two pumps phase-modulated 180 degrees out of phase. Section 2.4 states the problem and summarizes the results of our cancellation technique.

2.1.   Demonstration of FWC in Highly Nonlinear Dispersion-Shifted Fiber

In earlier experiments. FWCs were demonstrated in conventional dispersion-shifted fibers (DSFs). DSFs are designed for transmission rather than for FWC applications. and they have the following disadvantages for FWC applications: (1) a relatively low nonlinearity coefficient, $\gamma \cong 2 \text{ km}^{-1}\text{W}^{-1}$; and (2) a fairly large dispersion slope, $D_\lambda \cong 0.07 \text{ ps ?nm}^{-2}\text{km}^{-1}$. As a result of (1). for a given pump power P_0 the fiber length L required for gain > 10 dB is large. ranging from 200 m for a pulsed pump. to 12 km for a cw pump. And because of (1) and (2). appreciable bandwidth (10s of nm) can be

20

achieved only if the (pulsed) pump wavelength λ_p is within about 1 nm of the zero-dispersion wavelength λ_0 .

Recently, several fiber manufacturers started to develop highly-nonlinear dispersion-shifted fibers (HNLF). This type of fiber is designed to enhance nonlinear effects in fibers. The enhancements appear in two ways. First, the nonlinear coefficient is increased because of larger n_2 (nonlinear refractive index) and smaller effective area. Higher nonlinearity reduces the power or fiber length required to achieve the same gain. Second, the dispersion slope is reduced, resulting in a wider bandwidth [Marhic-a].

We are the first to demonstrate an FWC using HNLF. Figure 1 shows the experimental result. Further information can be found in [Ho-a].
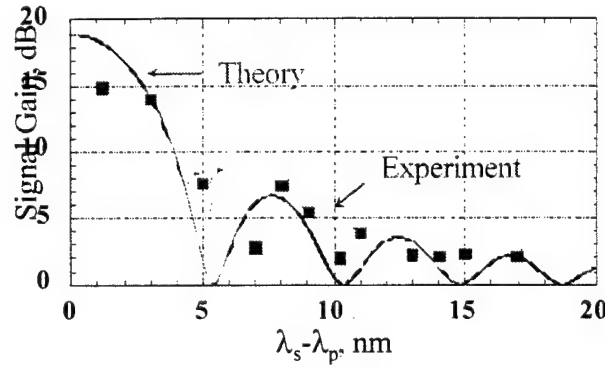

Figure 1: Experimental results for an FWC using HNLF.

2.2. FWC Bandwidth Expansion Using a Dispersion Compensation Technique

Although HNLFs have the desirable features for FWC applications, their zero dispersion wavelengths (λ_0 s) are not easy to control during manufacturing. For example, the HNLF presented in the first demonstration of FWC with HNLF (Section 2.1) has $\lambda_0 = 1591\ nm$. This is far from the wavelength region where high power pumping sources are currently available, i.e., 1530-1565 nm. With pump wavelength $\lambda_P = 1542\ nm$ in our experiment, the separation between λ_P and λ_0 is 49 nm, which results in an FWC with very small gain bandwidth. In order to solve this problem, we proposed a dispersion compensation method that involves splicing together pieces of fiber with dispersion of opposite signs at various locations in the HNLF. This compensated fiber has equivalent λ_0 closer to the pump wavelength.

We have performed theoretical studies [Marhic-b] to quantitatively analyze the feasibility of this technique. We also performed experiments [Ho-b] to confirm the

21

theory. In the experiments. we compensated the dispersion of HNLF by splicing pieces of fibers of opposite sign dispersion at various locations in the HNLF. The three composite fibers we constructed to demonstrate this technique are illustrated in Figure 2. Note that we use standard single-mode fiber (SMF) as the dispersion-compensating fiber (DCF) in our experiment. because it provides large positive dispersion ($D \cong 16.3 \, \text{ps} \, ?\text{nm}^{-1}\text{km}^{-1}$) in 1550 nm window. The pump is pulse-modulated to achieve 11 W peak power. The measured gain curves for all three composite fibers are plotted in Figure 3 along with theoretical curves. The results show that: (1) the experimental results agree well with the theory; and (2) the proposed dispersion compensating technique increases both FWC's conversion gain and bandwidth.
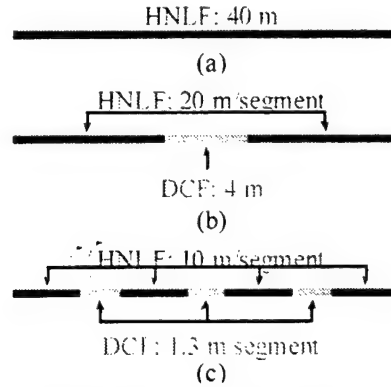

Figure 2: Assembly of the fibers: (a) HNLF only: (b) HNLF + 1 segment of DCF segment: (c) HNLF + 3 segments of DCF.
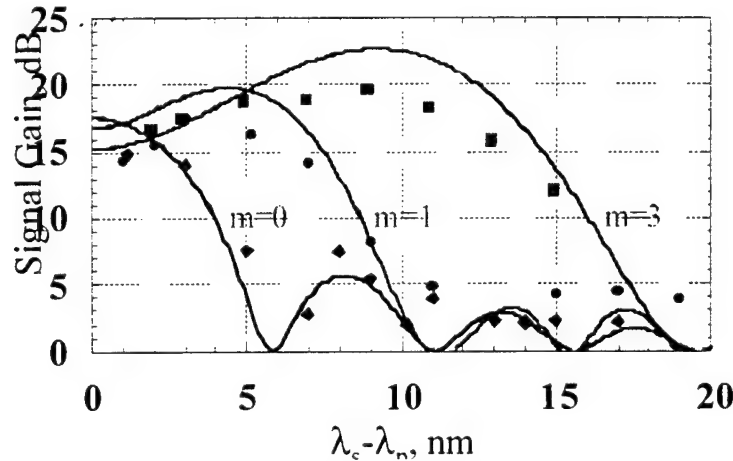

Figure 3: Gain measurements of pulsed one-pump FWCs with dispersion-compensated HNLFs. Solid lines are theoretical plots and dots are experimental data points. The m's denote the number of DCF segments.

2.3. Broadband FWC and Its Interaction with Raman Gain

Early work with FWCs demonstrated relatively small bandwidths, of the order of 1 nm. We have shown that under certain circumstances. FWCs could in principle exhibit bandwidths as large as several hundred nanometers [Marhic-a]. and we have experimentally demonstrated a 120 nm bandwidth FWC as part of this project [Ho-c].

We have continued this broadband FWC effort by studying theoretically and experimentally FWCs with a bandwidth of the order of 200 nm. Under these circumstances. the FWC bandwidth significantly overlaps the pump-induced Raman gain bandwidth, which peaks at about 110 nm from the pump. on the long wavelength side. It then becomes necessary to study the combined effect of the two separate gain mechanisms. We have studied the theory applicable to this regime. and also performed experiments to verify the theoretical predictions.

The gain medium for our OPA experiment was a highly nonlinear fiber (HNLF) provided by Furukawa Electric. Table 1 lists the HNLF parameters. As can be seen. the zero-dispersion wavelength λ_0 of this fiber is much closer to the available pump source. Therefore. an FWC with bandwidth over 200 nm is possible with this HNLF.

Table 1: HNLF parameters.

Parameter	Value
Zero dispersion wavelength λ_0	1540.2 nm
Dispersion slope D_λ (at λ_p)	0.031 ps ?nm^{-2} ?km^{-1}
Nonlinearity coefficient γ	18 km^{-1} ?W^{-1}
Length L	20 m
$\beta^{(4)}$ (at λ_p)	-5.8×10^{-56} s^4 ?m^{-1}

We first characterized the Raman gain of this HNLF. and the result is shown in Figure 4 (a). We then performed the pulsed-FWC experiment. and the results are shown in Figure 4 (b). In Figure 4 (b). the dashed curve marked "FWC only" shows the hypothetically pure FWC gain without Raman contribution. It is symmetric, whereas the experimental data exhibits asymmetry. with higher gain on the longer wavelength side, a feature clearly attributable to the Raman gain. The solid curve marked "FWC+Raman" is plotted with the Raman effect. The experimental data are in good agreement with this curve. indicating the validity of the model we developed. Note also that the two curves

("FWC only" and "FWC+Raman") confirm that the pump-induced Raman gain contribution is relatively small compared to the FWC gain.

In this work, we have demonstrated an FWC with gain in excess of 10 dB over a 208 nm bandwidth, which to our knowledge is the largest to date for any type of fiber-based wavelength converter. We also confirmed that the Raman gain provides only a relatively small perturbation to the broadband and high-efficiency FWC.
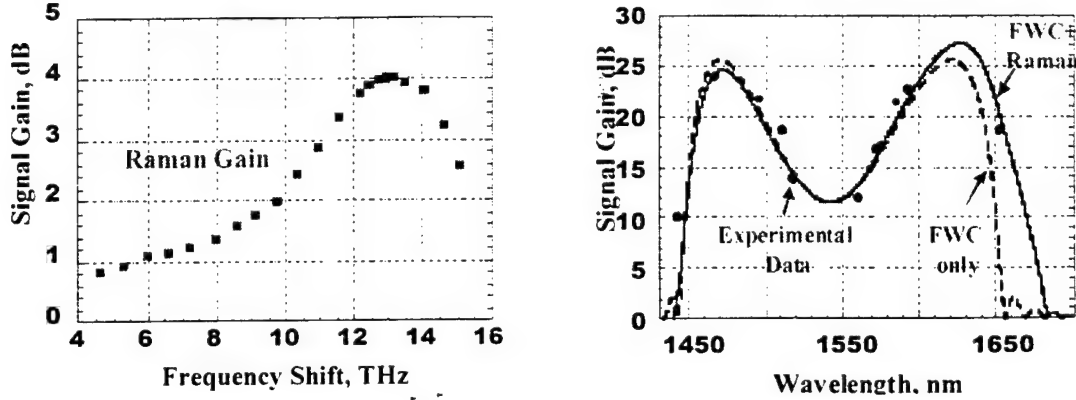

Figure 4: (a) Raman gain spectrum. The frequency shift is defined as the pump frequency minus the signal frequency. (b) Experimental results. The dots are experimental data, and the solid and dashed lines are theoretical curves obtained with and without the Raman effect.

2.4. Cancellation of Idler Broadening by Two-Pump FWCs

The efficiency and bandwidth of FWCs strongly depend on the pump power. Pump power levels of hundreds of milliwatts are currently necessary to achieve reasonable performance. Unfortunately, at this high power level, another nonlinear phenomenon, Stimulated Brillouin Scattering (SBS) also occurs. It causes reflection of most pump power, and thus reduces the pump power going through the fiber. SBS has been widely studied, and techniques have been proposed and demonstrated to suppress it. Since SBS has only a very narrow bandwidth, a common technique to suppress it is to artificially broaden the pump linewidth by modulating the pump. This process is called pump dithering. Either AM, FM, or PM can be used to achieve this goal. At high pump powers, pump broadening of several GHz may be required.

Although pump dithering suppresses SBS, it creates another problem, illustrated in Figure 5 (a). If ω_1 (pump) is shifted by $\Delta\omega$, then ω_4 (idler, or converted signal) is shifted by $2\Delta\omega$. As a result, the pump frequency dithering is transferred to the idler, multiplied by a factor of two. This leads to idler spectrum broadening of several GHz at high pump power.

24

To solve the idler linewidth broadening problem. a technique was proposed in [Yang]. The principle is shown in Fig. 1(b). Instead of using a one-pump configuration. a two-pump OPA [Marhic-c] is used. In a two-pump configuration, the idler broadening can be cancelled, when the two pumps are adjusted carefully. as illustrated in Fig. 1(b).
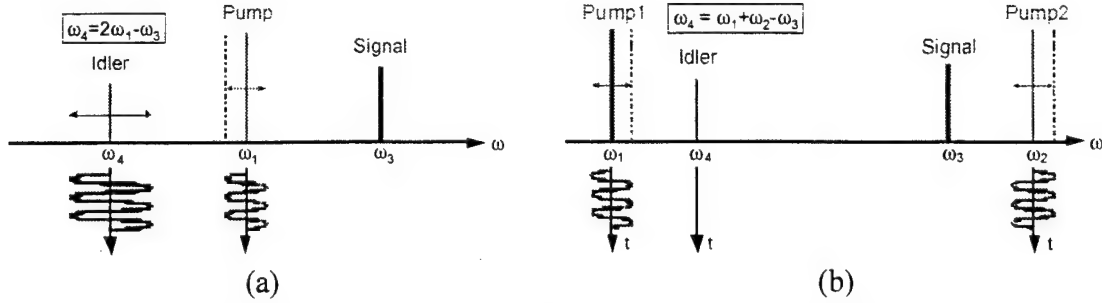
Figure 5: (a) Idler broadening due to pump dithering. (b) Idler broadening suppression using two-pump scheme.

We have theoretically investigated and experimentally implemented this technique by two different methods – FM modulation [Ho-d] and PM modulation [Ho-e]. Figure 6 shows part of the results of the cancellation experiment. Figure 6 (a) shows the idler spectrum when cancellation is applied. For comparison. Figure 6 (b) shows the idler spectrum when no cancellation is applied. The comparison shows that without cancellation, the modulation due to pump dithering is lower by 4 dB than the center peak, and that with cancellation, the modulation is 17 dB lower than the center peak. The spread of the sidebands is also reduced with cancellation. from 6 GHz to 2 GHz. Further results show that the idler can have almost the same quality as the output signal. This approach could help make fiber FWM- and OPA-based wavelength converters practical.

Figure 6: Results: (a) idler spectrum with broadening suppression; (b) idler spectrum without broadening suppression.

3 JSEP SUPPORTED PUBLICATIONS

1. F. S. Yang, M.-C. Ho, M. E. Marhic, and L. G. Kazovsky, "Demonstration of two-pump fiber optical parametric amplification," *LEOS'97*, paper MN4, vol. 1, pp. 122-123, San Francisco, CA, Nov. 10-13, 1997.
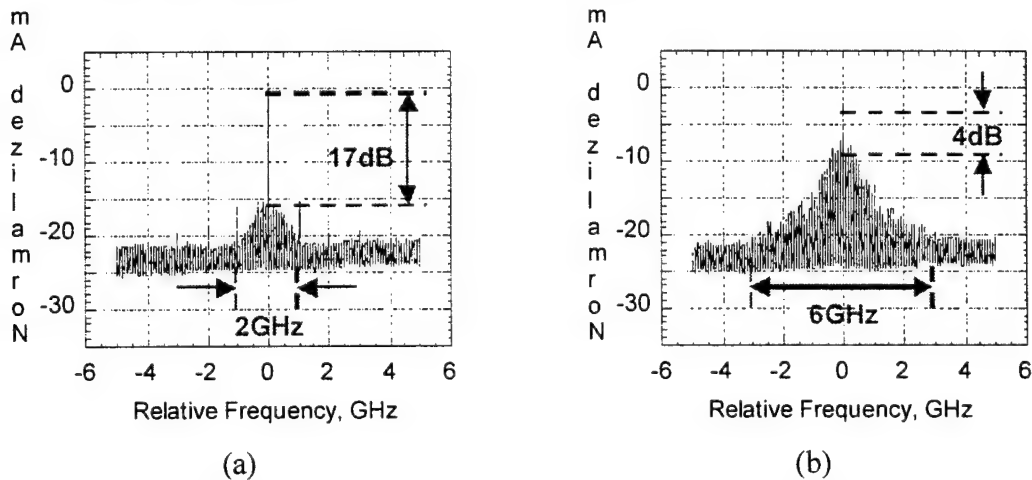
2. M.-C. Ho, F. S. Yang, M. E. Marhic, and L. G. Kazovsky, "Optical parametric amplification in a high-nonlinearity fiber," *CLEO'98*, paper CFA6, pp. 496-497, San Francisco, CA, May 3-8, 1998.

3. M.-C. Ho, F. S. Yang, M. E. Marhic, and L. G. Kazovsky, "Fiber optical parametric amplifier: bandwidth expansion by dispersion compensation," *LEOS'98*, paper ThG2, vol. 2, pp59-60, Orlando, FL, Dec. 1-4, 1998.

4. M.-C. Ho, F. S. Yang, M. E. Marhic, and L. G. Kazovsky, "Idler spectral broadening suppression in two-pump optical parametric amplifier," *Proceedings of the SPIE, ICO'99*, vol. 3749, pp. 96-97, San Francisco, CA, Aug. 2-6, 1999.

5. M.-C. Ho, M. E. Marhic, Y. Akasaka, F. S. Yang, and L. G. Kazovsky, "Fiber optical parametric amplifier with 120 nm bandwidth," *NLGW'99*, paper WB6, pp. 39-41, Dijon, France, Sept. 1-3, 1999.

6. M.-C. Ho, M. E. Marhic, Y. Akasaka, and L. G. Kazovsky, "Fiber optical parametric amplifier and wavelength converter with 208 nm gain bandwidth," *CLEO2000*, paper CThC6, pp. 401-402, San Francisco, CA, May 7-12, 2000.

7. F. S. Yang, M.-C. Ho, M. E. Marhic, and L. G. Kazovsky, "Demonstration of two-pump fiber optical parametric amplification," *Electron. Lett.*, vol. 33, no. 21, pp. 1812-1813, Oct. 9, 1997.

8. M. E. Marhic, F. S. Yang, M.-C. Ho, and L. G. Kazovsky, "High-nonlinearity fiber optical parametric amplifier with periodic dispersion compensation," *J. Lightwave Technol.*, vol. 17, no. 2, pp. 210-15, Feb. 1999.

9. M.-C. Ho, K. Uesaka, M. E. Marhic, Y. Akasaka, and L. G. Kazovsky, "200 nm-Bandwidth Fiber Optical Amplifier Combining Parametric and Raman Gain," *J. Lightwave Technol.*, July 2001.

10. M.-C. Ho, M. E. Marhic, K. Y. K. Wong, and L. G. Kazovsky, "Narrow-linewidth idler generation in fiber four-wave mixing and parametric amplification by dithering two pumps in opposition of phase," submitted for publication.

4   JSEP SUPPORTED DISSERTATION

Min-Chen Ho, *Fiber Optical Parametric Amplifiers and Their Applications in Optical Communication Systems*, Ph. D. dissertation, Stanford University, June, 2001.

5   REFERENCES

[Yoo]   S. J. B. Yoo, "Wavelength conversion technologies for WDM network applications," *J. Lightwave Technol.*, vol. 14, no. 6, pp. 955-966, June 1996.

[Willner]   A. E. Willner, M. C. Cardakli, O. H. Adamczyk, Y.-W. Song, and D. Gurkan, "Key building blocks for all-optical networks," *IEICE Trans. Commun.*, vol. E83-B, no. 10, pp. 2166-2177, Oct. 2000.

[Stubkjaer]   K. E. Stubkjaer, A. Klock, P. B. Hansen, H. N. Poulsen, D. Wolfson, K. S. Jepsen, A. T. Clausen, E. Limal, and A. Buxens, "Wavelength Converter Technology," *IEICE Trans. Commun.*, vol. E82-B, no. 2, pp. 390-400, Feb. 1999.

[Brener]   I. Brener, B. Mikkelsen, G. Raybon, R. Harel, K. Parameswaran, J. R. Kurz, M. M. Fejer, "160Gbit/s wavelength shifting and phase conjugation using periodically poled LiNbO3 waveguide parametric converter," *Electron. Lett.*, vol. 36, no. 21, pp. 1788-1790, Oct. 12, 2000.

[Watanabe]   S. Watanabe, S. Takeda, T. Chikama, "Interband wavelength conversion of 320 Gb/s (32x10 Gb/s) WDM signal using a polarization-insensitive fiber four-wave mixer," *ECOC'98*, vol. 3, pp. 83-87, Madrid, Spain, 20-24, Sept. 1998.

[Aso]   O. Aso, S. Arai, T. Yagi, M. Tadakuma, Y. Suzuki, S. Namiki, "Broadband four-wave mixing generation in short optical fibres," *Electron. Lett.*, vol. 36, no. 8, pp. 709-711, Apr. 13, 2000.

[Marhic-a]   M. E. Marhic, N. Kagi, T. K. Chiang, and L. G. Kazovsky, "Broadband fiber optical parametric amplifiers," *Opt. Lett.*, vol. 21, no. 8, pp. 573-5, April 1996.

[Sun] Y. Sun. J. W. Sulhoff. A. K. Srivastava. A. Abramov. T. A. Strasser. P. F. Wysocki. J. R. Pedrazzani. J. B. Judkins. R. P. Espindola. C.Wolf. J. L. Zyskind. A. M. Vengsarkar. and J. Zhou. "A gain-flattened ultra wide band EDFA for high capacity WDM optical communications systems." *ECOC'98*. vol. 1. pp. 53-54. Madrid. Spain. 20-24 Sept. 1998.

[Kani] J. Kani. K. Hattori. M. Jinno. T. Kanamori. and K. Oguchi. "Triple-Wavelength-Band WDM Transmission Over Cascaded Dispersion-Shifted Fibers." *IEEE Photon. Technol. Lett.*. vol. 11. no. 11. pp. 1506-8. Nov. 1999.

[Ho-a] M.-C. Ho. F. S. Yang. M. E. Marhic. and L. G. Kazovsky. "Optical parametric amplification in a high-nonlinearity fiber." *CLEO'98*. paper CFA6. pp. 496-497. San Francisco. CA. May 3-8. 1998.

[Marhic-b] M. E. Marhic. F. S. Yang. M.-C. Ho. and L. G. Kazovsky. "High-nonlinearity fiber optical parametric amplifier with periodic dispersion compensation." *J. Lightwave Technol.*. vol. 17. no. 2. pp. 210-215. Feb. 1999.

[Ho-b] M.-C. Ho. F. S. Yang. M. E. Marhic. and L. G. Kazovsky. "Fiber optical parametric amplifier: bandwidth expansion by dispersion compensation." *LEOS'98*. paper ThG2. vol. 2. pp59-60. Orlando. FL. Dec. 1-4. 1998.

[Ho-c] M.-C. Ho. M. E. Marhic. Y. Akasaka. F. S. Yang. and L. G. Kazovsky, "Fiber optical parametric amplifier with 120 nm bandwidth." *NLGW'99*, paper WB6. pp. 39-41. Dijon. France. Sept. 1-3. 1999.

[Yang] F. S. Yang. M. E. Marhic. and L. G. Kazovsky. "CW fiber optical parametric amplifier with net gain and wavelength conversion efficiency greater than one." *Electron. Lett.*. vol. 32. no. 25. pp. 2336-2338. Dec. 5, 1996.

[Marhic-c] M. E. Marhic. Y. Park. F. S. Yang. and L. G. Kazovsky. "Broadband fiber-optical parametric amplifiers and wavelength converters with low-ripple Chebyshev gain spectra". *Opt. Lett.*. vol. 21. no. 17, pp. 1354-1356, Sept. 1, 1996.

28

[Ho-d]   M.-C. Ho. F. S. Yang. M. E. Marhic. and L. G. Kazovsky. "Idler spectral broadening suppression in two-pump optical parametric amplifier." *Proceedings of the SPIE. ICO'99.* vol. 3749, pp. 96-97. San Francisco. CA. Aug. 2-6, 1999.

[Ho-e]   M.-C. Ho, M. E. Marhic, K. Y. K. Wong. and L. G. Kazovsky. "Narrow-linewidth idler generation in fiber four-wave mixing and parametric amplification by dithering two pumps in opposition of phase," submitted for publication.

Distributed Adaptive Signal Processing

Teresa H. Meng
Senior Investigator

Volkan Rodoplu & Mark Dzwonczyk
Graduate Students

Department of Electrical Engineering
Stanford University

This research continues to examine technologies for low-power, high-performance, reliable, and reusable architectures for distributed adaptive signal processing. The objective is to demonstrate a design methodology which is not only adaptable but also trainable with capability for massively parallel and distributed processing. It will integrate distributed network techniques and provide a design environment for automatic reconfiguration and rapid system prototyping.

I. Minimum Energy Network Protocol

A challenge in designing distributed networks is finding an efficient protocol for multiple access. The first issue that any such protocol must address is the temporal and or frequency separation of the transmit and receive slots of any node. This means either that a node must transmit and receive in different time slots or that it must transmit and receive on widely separated frequencies using filters with sharp out-of-band rejection.

This requirement presents a considerable challenge in a distributed network where the aim is peer-to-peer communications between geographically distributed nodes. For example, in a communication transmission from Node A to Node B, the system designer must insure that the receiver Node B is in the receive mode independent of the physical locations of Node A and Node B. Further, the designer must make this possible for every pair of nodes within a transmission range of each other.

We have a designed a position-based multiple access protocol which leverages two important technologies that have emerged recently:

(1) *Global Positioning System.* In our related DARPA-sponsored research, we have already demonstrated the viability of small, low-cost, low-power GPS receivers. A radio network architecture for this program uses the GPS position and absolute time information for both the estimation of transmit power fall-off with respect to distance and multiple access duplexing and user signature assignments. The former of these techniques was demonstrated in July 1998 while the latter is being demonstrated in our current research.

(2) *Multi-User Detection:* Low complexity multi-user detectors and interference cancelers are recent advances in the physical layer design of communication systems. In our multiple access protocol, we make use of these detectors at the receiver of each node to achieve high efficiency in spectrum usage.

Our position-based duplexing strategy allows the designer to trade-off spectral efficiency for multi-user communications with the fraction of the whole deployment region with which a node can communicate. The idea here is to divide up the deployment region into cells which are called *duplexing* cells. Each cell is assigned a different duplexing pattern which any node in that cell must use for its transmission and reception. An example for a duplexing pattern is {T,R,T,T,R,T,...}, where T denotes a Transmit slot and R denotes a Receive slot for that user. In the above example, the user must transmit in the first slot, receive in the second, transmit in the third and fourth slots, etc.

We have found an optimal duplexing scheme such that for a block consisting of such cells, each node in this block of cells can communicate with every other node in the same block in a manner that makes the best use of the available bandwidth.

In contrast to traditional multiple access protocols such as CSMA, our protocol allows users to transmit at the same time without collisions. Since traditional protocols do not use multi-user detection at the receivers, they cannot avoid collisions from taking place. In our protocol, which leverages multi-user detection, simultaneous reception from many users is possible.

The important point in this discussion is that the assignment of duplexing patterns and user signatures occur in a completely distributed fashion since these assignments are based on position. Each node knows its own position via the GPS, since there is a particular pre-assigned duplexing code and a pre-assigned family of user signatures for the cell in which the node is located, the node knows with which pattern and which signature to transmit.

We are currently simulating the position-based multiple access protocol (PBMA) in OPNET, which is a versatile network simulator.

II. Likelihood of System States for Non-Stationary Processes

In our last report, we described an approach that combines classical linear regression techniques with instantaneous error to define the likelihood that the coefficients of a linear predictor adequately capture a system's state. Such a method could be leveraged for monitoring complicated mechanical objects in real-time for signs of critical wear. For this research program, the end objective is to deploy numerous intelligent adaptive systems over a wide geographic area for data gathering, relying upon communication systems to integrate local processing into a distributed consensus. This approach -- when compared to conventional centralized systems -- increases performance, reduces latency and, most importantly, reduces the overall system cost. For this approach to work, however, each individual local processor must be labeled with a likelihood measure of correct operation.

Our work in the estimation of non-stationary time-series processes has resulted in a novel probability model that can assign a likelihood measure to accuracy of adaptive predictors. This model combines short-term error and long-term accumulated error to accommodate adaptation as a non-stationary process transpires.

For a linear predictor, the instantaneous error (e.g., Normalized Least Mean Squares) determines how well (or how poorly) the current coefficients capture the state of the system. One can view error in terms of a probability: as error increases, the system is likely to be moving from one state to another. If error is consistently high, a number of different states are likely. If error is low, the state is specified with a higher likelihood. Thus the error is directly proportional to predictor performance. One can build a probability density model based upon this error to quantitatively determine the relationship between error and performance.

31

In a complementary fashion, linear regression techniques can be used to describe the long-term confidence in the predictor coefficients. An accumulated sum-of-squares error is the basis for confidence intervals on a system's regressors, which, in this case, are the predictor coefficients themselves. A system with large accrued error is not being modeled well and will result in large confidence intervals on its regressors. Similar to the instantaneous error situation, a probability density model based upon confidence interval size can be built that explicitly depicts the relationship between error and performance.

Our novel approach integrates both of the probability models to form a multi-dimensional joint probability density. This model allows one to determine the probability of "correct prediction" as a function of instantaneous error and regressor confidence intervals. Since confidence intervals are defined on individual regressors, or confidence hyper-volumes are defined on the vector of regressors, the density function is truly multi-variate. In the model, all parameters are normalized (between 0 and 1).

Combining the probability measure in this framework of a "state space road-map" means that it can be used as a instantaneous confidence measure of route that the system proceeds upon within that space. Simulation results have provided preliminary validation of the mathematical bases for the models. Real-world validation is being pursued by applying the method to the prediction of the vibration signature of rotor-craft gear-boxes (transmissions) as they mechanically fail. Actual data from US Navy drive-train test-stands are used to validate the method and underlying assumptions.

We believe the approach has much broader application in the general field of state identification for non-stationary processes. For example, in a communication system, the joint probability density can be used for channel identification. Where channels are highly non-stationary, e.g., mobile telephony, a reliable estimate of the channel configuration can be used to increase capacity and reduce power consumption of both the transmitter and receiver.

TITLE: Efficient Data Compression

PRINCIPAL INVESTIGATOR: Thomas M. Cover

GRADUATE STUDENTS DIRECTLY SUPPORTED BY JSEP:
Assaf Zeevi (Ph.D. '01), Joshua Singer, Arak Sutivong, and
Young-Han Kim

AFFILIATED STUDENTS:
Ioannis Kontoyiannis (Ph.D. '98), Garud Iyengar (Ph.D. '98),
Suhas Diggavi (Ph.D. '98), David Julian,
and Gleb Klimovitch

1   Scientific Objectives

We apply techniques of information theory to problems of information compression, network information flow, investment, and quantum data transmission. The investigations cover the following specific areas:

1. Universal lossy compression

2. Optimal signaling under the worst noise

3. Characterizing and estimating rare events

4. Duality between channel coding and source coding with side information

5. Transmission over channel with side information

6. Optimal investment

7. Quantum multiple-access channel

2   Summary of Research

2.1   Universal Lossy Compression

We address a long-standing open problem in data compression, that of finding an efficient extension of the celebrated Lempel-Ziv algorithm to the case of *lossy* compression. In [Kontoyiannis I] we present a universal algorithm for encoding memoryless sources at a fixed distortion level, which arises as a generalization of the Lempel-Ziv lossless compression scheme to the lossy case. We show that the compression performance of the proposed scheme is asymptotically optimal with respect to bounded single-letter distortion measures, and argue that it is of reasonable encoding complexity. The main result is related to the results in the papers [Kontoyiannis II] and [Kontoyiannis III].

2.2 Signaling Under the Worst Noise

In this work [Diggavi and Cover] we find the worst constrained noise processes for the additive noise channel. If the signal and noise covariances matrices lie in bounded convex sets, we show that a random Gaussian codebook and a decoding scheme based on a Gaussian metric achieve the minimax rate. We demonstrate the solution to the game-theoretic problem when we have a banded matrix constraint (specified up to a certain covariance lag) on the noise covariance matrix and show that under certain conditions (sufficient input power) the maximum entropy noise is also the solution to the minimax problem.

2.3 Characterizing and Estimating Rare Events

In many application areas ranging from manufacturing, supply chains, communication networks and financial engineering, intrinsic variability causes various risk and reliability concerns. Typically, an attempt is made to mitigate risk to a certain degree. Consequently, in many cases variability caused violations become something of a "rare event." In this work [Zeevi and Glynn] and [Zeevi] we consider certain aspects of extreme value theory and the role it plays in the analysis of atypical system behavior. Specifically, we discuss how extreme values might be useful in characterizing these so-called rare events, while "extremal statistics," estimators based on extreme values, can be used in estimating and predicting their occurrence.

2.4 Duality Between Channel Coding and Source Coding With Side Information

In [Chiang and Cover I] and [Chiang and Cover II] we show that the duality between channel capacity and data compression is retained when state information is available to the sender, to the receiver, to both, or to neither. We also present a unified theory for eight special cases of channel capacity and rate distortion with state information, which extends existing results to arbitrary pairs of i.i.d state information (S_1, S_2) available at the sender and at the receiver, respectively. We also show that the general formula of channel capacity assumes the same form as the Wyner-Ziv rate distortion function with state information.

2.5 Transmission Over Channel With Side Information

In [Costa] Costa showed that the capacity of a channel with additive white Gaussian noise and power constrained input is not affected if some extra i.i.d noise sequence is added to the output of the channel, as long as the full knowledge of this extra noise sequence is given to the encoder. In this work [Yu, et al] we generalize Costa's result to the case where the additive noise is colored and not necessarily stationary or ergodic. We show that the capacity for such a channel is also not affected by the extra additive noise sequence.

In related work [Chiang, Sutivong, and Cover], we study a conflict between transmitting pure information and state information over a channel where the transmitter has a complete knowledge about the state of the channel. The novelty in characterizing the tradeoff between transmitting pure information and state information arises primarily because of the inability to encode and decode the state information. The tradeoff region is typically difficult to

obtain even for a simple channel. In [Sutivong, Chiang, and Cover] we characterize the optimal tradeoff for the binary channel and also prove the optimality of the extreme points of the tradeoff region for the additive Gaussian channel.

2.6 Optimal Investment

In [Cover and Julian] we compare the theoretical and empirical performance of horizon-free universal portfolio for a large number of stock pairs using real stock market data. We consider two scenarios: with and without side information, and with and without short selling. We also derive a correction factor for the asymptotic performance of the universal portfolio. Finally, we propose the concept of a parallel artificial market and show empirically that maximum likelihood with prepending provides a computationally efficient method to compute the universal portfolio.

In related work [Iyengar and Cover], we formulate the problem of growth optimal investment in horse race markets with proportional costs and study growth optimal strategies for both stochastic horse races as well as races where one does not make any distributional assumptions. Our result extends all known results on frictionless horse race markets to their natural analog in markets with costs.

2.7 Quantum Multiple-access Channel

In [Klimovitch] we analyze a quantum adder channel, i.e. the extension of a classical multiple-access additive binary channel to the quantum regime, in which quantum bits (qubits) rather than classical bits are transmitted. Quantum entanglement between different trasmitters and the receiver results in a significant expansion of the capacity region of the channel in comparison with its classical counterpart. For two uncoordinated users, the maximum rate of a single user doubles, while the maximum rate-sum increases by a factor larger than two.

References

[Kontoyiannis I] I. Kontoyiannis, "An implementable lossy version of the Lempel-Ziv algorithm – Part I: Optimality for memoryless sources," *IEEE Transactions on Information Theory*, 45, pp. 2293-2305, Nov. 1999.

[Kontoyiannis II] I. Kontoyiannis, "Asymptotic recurrence and waiting times for stationary processes," *Journal of Theoretical Probability*, 11, pp. 795-811, July 1998.

[Kontoyiannis III] A. Dembo and I. Kontoyiannis, "The asymptotics of waiting times between stationary processes, allowing distortion," *Annals of Applied Probability*, 9, pp. 413-429, May 1999.

[Diggavi and Cover] S.N. Diggavi and T.M. Cover, "Is maximum entropy noise the worst?," *Proceedings of the IEEE International Symposium on Information Theory 1997, Ulm, Germany*.

[Zeevi and Glynn] Zeevi. A.J. and Glynn. P.W.. "On the maximum workload of a queue fed by fractional Brownian motion."*Ann. of Appl. Probab..* 2001.

[Zeevi] Zeevi, A. "On the accuracy of estimating tail probabilities in queues" *Proceedings of International Symposium on Information Theory.* IEEE press. Eds. Ezio Biglieri and S. Verdu, 2000.

[Yu, et al] W. Yu. A. Sutivong, D. Julian. T. M. Cover. and M. Chiang. "Writing on colored paper." *accepted to appear in IEEE International Symposium on Information Theory.* Washington D.C., June 2001.

[Costa] Max H. M. Costa. "Writing on dirty paper." IT-29:439-411, May 1983.

[Chiang, Sutivong, and Cover] M. Chiang. A. Sutivong, and T. M. Cover, "Channel capacity and state estimation," *Proceedings of IEEE International Symposium on Information Theory and Applications*, Honolulu, Hawaii, November 2000, pp. 838-840.

[Sutivong, Chiang, and Cover] A. Sutivong. T. M. Cover, and M. Chian. "Tradeoff between message and state information rates," *accepted to appear in IEEE International Symposium on Information Theory*, Washington D.C., June 2001.

[Cover and Julian] T. M. Cover and D. Julian. "Performance of universal portfolios in the stock market," *Proceedings of IEEE International Symposium on Information Theory*, Sorrento, Italy, June 2000, p. 232.

[Klimovitch] G. Klimovitch, "On the classical capacity of a quantum multiple-access channel," *Proceedings of IEEE International Symposium on Information Theory*, Washington D.C., June 2001.

[Iyengar and Cover] G. Iyengar and T. M. Cover, "Growth optimal investment in horse race markets with costs,". *IEEE Transactions on Information Theory*, Nov. 2000, vol. 467, pp. 2675-2683.

[Chiang and Cover I] M. Chiang and T. M. Cover, "Duality of channel capacity and rate distortion with state information," *Proceedings of IEEE International Symposium on Information Theory*, Washington D.C., June 2001.

[Chiang and Cover II] M. Chiang and T. M. Cover, "Duality between channel capacity and rate distortion with state information and the Wyner-Ziv formula," *under review by IEEE Transactions on Information Theory*, 2001.

3 Publications Supported by JSEP

3.1 Ph.D. Theses Supported by JSEP

1. I. Kontoyiannis, "Recurrence and Waiting Times in Stationary Processes, and their Applications in Data Compression," May 1998.

2. G.N. Iyengar, "Analysis of Growth Rate of Wealth with Transaction Costs," June 1998.

3. A. Zeevi, "Extreme Values in Characterizing and Estimating Rare Events," June 2001.

3.2 Published Papers Supported by JSEP

1. T. M. Cover and E. Ordentlich. The equivalence of optimal market gain and minimax regret universal portfolios. *Proceedings of IEEE International Symposium on Information Theory*, June 1997, Ulm, Germany, p. 282.

2. E. Erkip and T. M. Cover. The initial efficiency of investment for the general market. *Proceedings of 1997 IEEE International Symposium on Information Theory*. June 1997. Ulm, Germany, page 283.

3. I. Kontoyiannis. Second-order noiseless source coding theorems. *IEEE Transactions on Information Theory*, 43, pp. 1339-1341, July 1997

4. I. Kontoyiannis. Second-order analysis of lossless and lossy versions of Lempel-Ziv codes. In *Proceedings of the 31st Asilomar Conference on Signals, Systems and Computers*, Pacific Grove, CA, November 1997.

5. I. Kontoyiannis, P.H. Algoet, Yu. M. Suhov and A.J. Wyner. Nonparametric entropy estimation for stationary processes and random fields, with applications to English text. *IEEE Transactions on Information Theory*, 44, pp. 1319-1327, May 1998.

6. E. Erkip and T. M. Cover. The Efficiency of Investment Information. *IEEE Transactions on Information Theory*, 4(3):1026-1040, May 1998.

7. I. Kontoyiannis. Asymptotic recurrence and waiting times for stationary processes. *J. Theoret. Probab.*, 11, pp. 795-811, July 1998.

8. T. M. Cover. Comments on Broadcast Channels. *IEEE Transactions on Information Theory*, 44(6):2524-2530, October 1998.

9. E. Ordentlich and T. M. Cover. The Cost of Achieving the Best Portfolio in Hindsight. *Mathematics of Operations Research*, 23(4):960-982, November 1998.

10. A. Dembo and I. Kontoyiannis. The asymptotics of waiting times between stationary processes, allowing distortion. *Ann. Appl. Probab.*, 9, pp. 413-429, May 1999.

11. I. Kontoyiannis. An implementable lossy version of the Lempel-Ziv algorithm – Part I: Optimality for memoryless sources. *IEEE Transactions on Information Theory*, 45, pp. 2293-2305, Nov. 1999.

12. T. M. Cover and D. Julian. Performance of Universal Portfolios in the Stock Market. *Proceedings of IEEE International Symposium on Information Theory*, Sorrento, Italy, June 2000, p. 232.

13. A. Sutivong, T. M. Cover, and M. Chiang. Tradeoff Between Message and State Information Rates. *Proceedings of IEEE International Symposium on Information Theory*, Washington D.C., June 2001.

3.3 Papers Submitted for Publication

1. S. Diggavi and T. M. Cover. The Worst Additive Noise Under a Covariance Constraint. *to appear in IEEE Transactions on Information Theory*. September 2001.

2. M. Chiang and T. M. Cover. Duality Between Channel Capacity and Rate Distortion with State Information and the Wyner-Ziv Formula. *under review by IEEE Transactions on Information Theory*, 2001.

ROBUST ADAPIVE FILTERING ALGORITHMS

PRINCIPAL INVESTIGATOR: T. Kailath
GRADUATE STUDENT: B. Halder

For the period 1/98 - 6/98 we concentrated on developing various robust algorithms for signal processing and communication applications. This is a continuation of the work reported earlier for the period 5/97 - 12/97. The main focus of the study was to extend the mixed H^2/H^∞ algorithms developed for the static state-feedback case as reported earlier to more general settings in order to include the following cases:

- Fixed order dynamic state-feedback.

- Fixed order output feedback.

This work was completed by Ph.D. student B. Halder who graduated in June 1998. Some publications on this are under review.

1 Mixed H^2/H^∞ Estimation and Control

The mixed H^2/H^∞ approach to controller design is an attempt to incorporate optimal performance and guaranteed robustness, arguably the two most desirable properties, into a single controller. In H^2 design a quadratic performance criterion is minimized under the assumption that an underlying model of the system and the statistical nature of the exogenous signals are known. As a result, the performance of the optimal H^2 controllers is susceptible to model uncertainties. In the H^∞ approach such assumptions are not made, and a minimax-type of criterion is adopted; however, the solutions may be over-conservative in terms of the H^2 performance. Fortunately, given an upper bound on the H^∞ performance there is a multiplicity of H^∞ controllers, and in the mixed approach we exploit this multiplicity to obtain a controller with the optimal H^2 performance subject to an H^∞ bound. To pose the mixed H^2/H^∞ problem as a contained optimal control problem, consider the general 2-input 2-output LTI system model show in Figure 1.
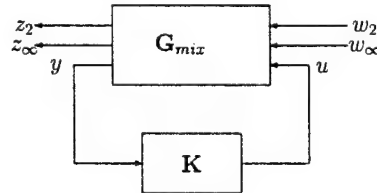

Figure 1: System model for the mixed H^2/H^∞ problem.

Mixed H^2/H^∞ Problem: Given the system $\mathbf{G}_{mix}$, the goal of mixed H^2/H^∞ approach is to find a controller $\mathbf{K}$, if it exists, such that the H^2 norm of the closed-loop map from input w_2 to z_2 is minimized subject to a pre-specified bound (γ) on the H^∞ norm of the closed-loop map from input w_∞ to z_∞.

As it turns out, the mixed H^2/H_∞ problem, though easy to motivate, is surprisingly hard to solve analytically. Thus, despite its importance and considerable progress in robust control theory the mixed H^2/H_∞ problem by and large remains an open problem. In the absence of complete analytic solution to the mixed H^2/H^∞ problem, the need for efficient numerical algorithms is apparent. In the earlier work we developed efficient numerical algorithms for computing the optimal mixed controller for the static state-feedback case. In this report we present algorithm for more general setting, i.e., the dynamic state-feedback case and output feedback case.

As a first step towards the development of such algorithms, the design of the optimal mixed problem must be reformulated in a finite dimensional optimization framework. The size of the resulting optimization problem is determined by the order of the optimal mixed controller. However, a solution to the optimal mixed problem is not guaranteed to be of bounded order, let alone of a fixed-order. It is hard to formulate a finite dimensional optimization problem to obtain such variable order, possibly infinite order, solutions. This suggests the need to put some restriction on the controller order. We pose this restriction on the controller order by considering only the so-called *fixed-order* solutions where the order of the controller is pre-specified. By restricting the search to controllers of fixed-order, we obtain a meaningful finite dimensional constrained optimization problem.

The steps required for the formulation of the optimization problem are as follows. Using the state-space description, we represent the set of fixed-order controllers by a set of fixed size matrices. For convenience, the system matrices are stacked into a single design variable K. Next, the H^2 norm of the closed-loop map $T_{z_2 w_2}$ is expressed as an explicit function of the design variable K, and the H^∞ norm bound on the closed-loop map $T_{z_\infty w_\infty}$ is expressed as a bilinear matrix inequality (BMI) in the design variable K and a Riccati variable X. Using these expressions, the design of fixed-order mixed controllers is converted into a problem of minimization of the H^2 cost function subject to a BMI constraint. Both the H^2 cost function and the H^∞ constraint set expressed as BMI are non-convex in the design parameter K. There is no one-step method for solving this non-convex constrained minimization problem and we propose an iterative approach.

The key idea behind these iterative algorithms is to break the difficult non-convex problem into a series of subproblems that can be readily solved. Toward this goal we construct subproblems that are convex and hence, easily solvable. Convex subproblems are derived from the original problem by replacing the non-convex H^2 cost function by a quasi-convex upper bound and the non-convex constraint set, expressed as a BMI, by a convex inner approximation with an LMI description. Moreover, we show that these subproblems can be converted to a special class of

convex problems, known as semidefinite programming (SDP) problems, for which there are efficient algorithms available.

To illustrate the performance improvement achieved by fixed order dynamic mixed controller over the conventional central controller we consider a 3-ed order LTI system [3, 1]. The H^2 norm of the closed-loop map $T_{z_2 w_2}$ is plotted as a function of H^∞ bound γ and shown in Figure 2. Figure 2 also shows the H^2 norm corresponding to the central and the static mixed controller. The plot shows that the dynamic full-order state-feedback controller yields lower H^2 norm compared to the static controller, especially for the smaller values of γ close to the optimal H^∞ norm γ_{opt}. This is a significant difference between the mixed H^2/H^∞ problem and the optimal H^2 or the suboptimal H^∞ problems.
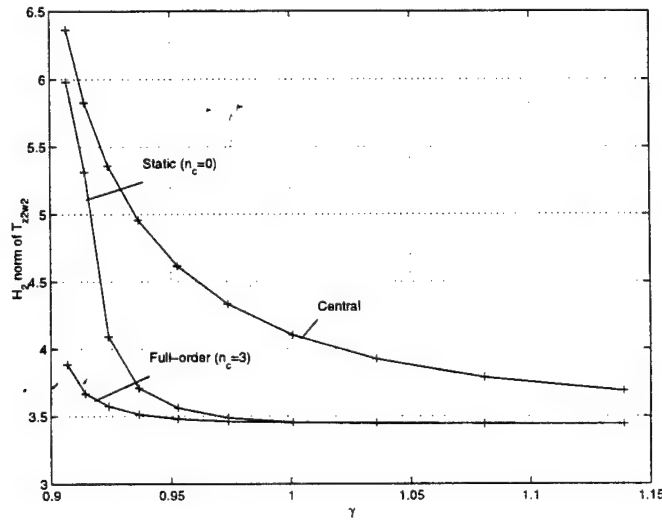

Figure 2: Algorithm-IV: H^2 performance of full-order ($n_c = 3$) dynamic controller (Example 5).

Using similar ideas we also developed algorithm for both static and fixed-order dynamic output feedback cases. For more details on these algorithms see [2].

41

References

[1] Halder, B. and Kailath, T. (1999) LMI Based Design of Mixed H_2/H_∞ Controllers: The State-Feedback Case, In *Proc. ACC June '99*.

[2] Halder, B. (1998), Design of optimal mixed H_2/H_∞ controllers, *Ph.D. Dissertation* . Stanford University.

[3] Halder, B. and Kailath, T. (1998) LMI Based Design of Mixed H_2/H_∞ Controllers: The State-Feedback Case, *Submitted for publication in Automatica*.

Scientific Personnel Supported by this Project
J. S. Harris, JSEP Director

Students
D. Stewart
B. Shimbo
T. Kramer
K. Gilbert
M.-C. Ho
V. Rodoplu
M. Dzwonczyk
A. Zeevi
J. Singer
A. Sutivong
Y.-H. Kim
B. Halder

JSEP Supported Publications
1. D. R. Stewart, D. Sprinzak, C. M. Marcus, C. I. Duruöz and J. S. Harris, Jr., *Science* **278**, 1784 (1997).

2   S. R. Patel, S. M. Cronenwett, D. R. Stewart, A. G. Huibers, C. M. Marcus, C. I. Duruöz, J. S. Harris, K. Campmana and A. C. Gossard, *Phys. Rev. Lett.* **80**, 4522 (1998).

3. A. G. Huibers, S. R. Patel, C. M. Marcus, P. W. Brouwer, C. I. Duruöz and J. S. Harris Jr., *Phys. Rev. Lett.* **80**, (1998).

4. M.-C. Ho, F. S. Yang, M. E. Marhic, and L. G. Kazovsky, "Optical Parametric Amplification in a High-Nonlinearity fiber," CLEO'98, pp. 496-7, May 1998.

5. M.-C. Ho, F. S. Yang, M. E. Marhic, and L. G. Kazovsky, "Fiber Optical Parametric Amplifier: Bandwidth Expansion by Dispersion Compensation," LEOS'98 11th Annual Meeting, Vol. 2, pp. 59-60, December 1998.

6. M.-C. Ho, F. S. Yang, M. E. Marhic, and L. G. Kazovsky, "Idler Spectral Broadening Suppression in Two-pump Optical parametric Amplifier," SPIE ICO XVIII, August 1999.

7. M.-C. Ho, M. E. Marhic, Y. Akasaka, F. S. Yang, and L. G. Kazovsky, "Fiber Optical Parametric Amplifier with 120 nm Bandwidth," NLGW'99, Submitted for publication.

8. M. E. Marhic, F. S. Yang, M.-C. Ho, and L. G. Kazovsky, "High-Nonlinearity Fiber Optical Parametric Amplifier with Periodic Dispersion Compensation," IEEE/OSA Journal of Lightwave Technology, Vol. 17, No. 2, pp. 210-5, February 1999.

9. E. Erkip and T. M. Cover, "The Efficienty of Investment Information, *IEEE Trans. On Info. Theory*, May 1998.

10. I. Kontoyiannis, "Asymptotically Optimal Lossy Lempel-Ziv Coding, *1998 IEEE International Symposium on Information Theory*, Cambridge, MA, August 1998.

11. I. Kontoyiannis, "On the Distribution of Recurrence Times and the Exact Asymptotics of Lempel-Ziv Coding," in *Proc. Of the 1997 IEEE Intl Symp. On Information Theory*, Ulm, Germany, June-July 1997.

12. I Kontoyiannis, "Two Refinements to Shannon's Source Coding Theorem, *IEEE Thans. On Info. Theory*, July 1997.

13. A. Zeevi and A. Goldenshluger, "Non-asymptotic Bounds for Autoregressive Approximations, *Proc. Of IEEE Intl. Symp. On Information Theory*, Cambridge, MA, August 1998.

14. A. Zeevi, "On Vector Quantizers Empirically Designed from Dependent Sources, in *Proc. Of the 1998 Data Compression Conf,* in Snowbird, UT, March-April, 1998.

JSEP Supported Dissertations

1. I. Kontoyiannis, *"Recurrence and Waiting Times in Stationary Processes and their Applications in Data Compression,"* Stanford University (1998)
2. G. N. Iyengar, *"Analysis of Growth Rate of Wealth with Transaction Costs,"* Stanford University (1998)
3. D. R. Stewart, "Level spectroscopy of Quantum Dots", Stanford University (1998).
4. M.-C. Ho, *Fiber Optical Parametric Amplifiers and Their Applications in Optical Communication Systems*, Stanford University. 2001.
5. A. Zeevi, *Extreme Values in Characterizing and Estimating Rare Events,"* Stanford University (2001)

Honors/Awards/Degrees
Ph.D. Degrees

1. D. R. Stewart, 1998
2. I. Kontoyiannis, 1998
3. G. N. Iyengar, 1998
4. M.-C. Ho, 2001
5. A. Zeevi, 2001

Inventions
None

Technology Transfer
None

REPORT DOCUMENTATION PAGE

Public Reporting burden for this collection of information is estimated to average 1 hour per response, including the time for reviewing instructions, searching existing data sources, gathering and maintaining the data needed, and completing and reviewing the collection of information. Send comment regarding this burden estimates or any other aspect of this collection of information, including suggestions for reducing this burden, to Washington Headquarters Services, Directorate for information Operations and Reports, 1215 Jefferson Davis Highway, Suite 1204, Arlington, VA 22202-4302, and to the Office of Management and Budget, Paperwork Reduction Project (0704-0188,) Washington, DC 20503.

1. AGENCY USE ONLY (Leave Blank)	2. REPORT DATE **March 31, 2001**	Final Progress Report: 05/01/97-03/31/01
4. TITLE AND SUBTITLE Proposal for Extension of JSEP Contract		DAAG55-97-1-0115
6. AUTHOR(S) J. S. Harris		
Stanford University		8. PERFORMING ORGANIZATION REPORT NUMBER
9. SPONSORING / MONITORING AGENCY NAME(S) AND ADDRESS(ES) U. S. Army Research Office P.O. Box 12211 Research Triangle Park, NC 27709-2211		10. SPONSORING / MONITORING AGENCY REPORT NUMBER 36290.1-EL-JSE

11. SUPPLEMENTARY NOTES

The views, opinions and/or findings contained in this report are those of the author(s) and should not be construed as an official Department of the Army position, policy or decision, unless so designated by other documentation.

12 a. DISTRIBUTION / AVAILABILITY STATEMENT Approved for public release; distribution unlimited.	12 b. DISTRIBUTION CODE

13. ABSTRACT (Maximum 200 words) This is the Final Report of the research conducted at Stanford Electronics Laboratories under the sponsorship of the Joint Services Electronics Program from May 1, 1997 through March 31, 2001. This report summarizes the areas of research, identifies the most significant results and lists the dissertations, publications and presentations sponsored by the contract (DAAG55-97-1-0115).

14. SUBJECT TERMS			15. NUMBER OF PAGES 43
			16. PRICE CODE

17. SECURITY CLASSIFICATION OR REPORT **UNCLASSIFIED**	18. SECURITY CLASSIFICATION ON THIS PAGE **UNCLASSIFIED**	19. SECURITY CLASSIFICATION OF ABSTRACT **UNCLASSIFIED**	20. LIMITATION OF ABSTRACT **UL**

NSN 7540-01-280-5500

RECEIVED

SEP 1 9 2001
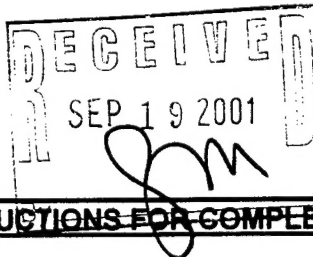
GENERAL INSTRUCTIONS FOR COMPLETING SF 298

The Report Documentation Page (RDP) is used for announcing and cataloging reports. It is important that this information be consistent with the rest of the report, particularly the cover and title page. Instructions for filling in each block of the form follow. It is important to *stay within the lines* to meet *optical scanning requirements.*